On Radiated Performance Evaluation of Massive MIMO Devices in Multi-Probe Anechoic Chamber OTA Setups

Kyösti, Pekka; Hentilä, Lassi; Fan, Wei; Lehtomaki, Janne; Latva-aho, Matti

Published in:
I E E E Transactions on Antennas and Propagation

DOI (link to publication from Publisher):
10.1109/TAP.2018.2860635

Publication date:
2018

Document Version
Accepted author manuscript, peer reviewed version

On Radiated Performance Evaluation of Massive MIMO Devices in Multi-Probe Anechoic Chamber OTA Setups

Pekka Kyösti, Lassi Hentilä, Wei Fan, *Member, IEEE,* Janne Lehtomäki, *Member, IEEE,* and Matti Latva-aho *Senior Member, IEEE*

***Abstract*—Radiated testing of massive multiple-input-multiple-output (MIMO) devices in fading radio channel conditions is expected to be essential in development of the fifth generation (5G) base stations (BS) and user equipment (UE) operating at or close to the millimetre wave (mm-wave) frequencies. In this paper we present a setup upgrading the multi-probe anechoic chamber based system designed originally for 4G UE. We describe methods for mapping radio channel models onto the probe configuration and discuss the differences to the former 4G case. We also propose metrics to assess the accuracy of the test setup and find key design parameters by simulations. The results with the utilized channel models indicate that at 28 GHz up to 16×16 planar arrays can be tested with range length of one meter and with at minimum eight active dual polarized probes.**

***Index Terms*—Antenna arrays, Anechoic chambers (electromagnetic), antenna measurements, fading channels, millimeter wave radio propagation, MIMO systems, testing.**

I. Introduction

New wireless telecommunication system, containing a multitude of new technology components, new frequency bands to be utilized, and new radio devices, is currently developed intensively. The purpose of the new system, commonly labelled as 5G, is to serve more devices, to enable higher data rates, lower latency, lower energy consumption, and to offer many other advanced and desirable features [1], [2].

Of the wide palette of 5G features the special interest to this paper is the combination of mm-wave frequency bands and massive MIMO antenna arrays. Sufficient wide bandwidths to support for mobile broadband data transfer are not available at the legacy cellular bands below 6 GHz. Thus new bands are now investigated from 24 GHz and higher [3], despite the transmission loss challenges inherent to the higher bands. Especially the frequencies around 28 GHz are considered for the so called pre-5G systems [4].

Massive MIMO technology is seen as a promising technology to enable high rate transmission to a large number of users in a dense network, and to compensate the severe transmission losses by substantial array gains [5]. Many experiments with massive MIMO arrays have been reported in the literature [6], [7] and the first commercial base station products are in a development phase. The expected mode of operation of large antenna arrays is the hybrid beamforming. For practical reasons, mainly related to the power consumption of components, each of the tens or hundreds antenna elements may not be supported by separate radio frequency (RF) chains. Instead the arrays may be connected to a base band unit by only a small number, e.g. eight, of RF chains. The antenna elements are divided to sub-arrays, where elements are combined to a single RF port by an analog weighting matrix. The matrix enables composing a predefined set of fixed antenna beams [4]. Thus each RF port, feeding a number of antenna elements (sub-array), may compose a number of predefined beam shapes. Typically main directions of a set of beams cover the angular sector of interest. In the link establishment the beam allocation and beam alignment are crucial operations to be tested.

One identified challenge on the development work is the testing of mm-wave massive MIMO devices. In [8] is predicted that the testing will move almost exclusively to radiated methods for a number of reasons. It is seen that the mm-wave devices are small in size and will be highly integrated units. Thus they may not provide RF connectors necessary for conducted testing. Even if they did, the number and the overall complexity of coaxial cable connections to test devices would increase impractical high. Attaching and detaching, e.g., one hundred coaxial cables is a time consuming and an error prone operation. Moreover, with massive MIMO the antenna characteristics and the analog array control are essential, thus it is crucial to test them altogether in a realistic manner with emphasis on the spatio-polarimetric propagation environment. For example testing the beam acquisition capability of massive MIMO devices, which is an initial step in link establishing procedure, will require emulating a spatio-polarimetric propagation environment.

OTA test methods for MIMO capable mobile terminals have been developed and researched for many years [9], [10]. The three main categories of methods are the reverberation chamber (RC) [11], the radiated two-stage (RTS) [12], and the multi-probe anechoic chamber based (MPAC) method [13]. Outside the referred standard documents has been introduced also a fourth option; reconfigurable OTA chamber [14], an RC whose walls are lined with antennas, supporting for reconstruc-

P. Kyösti is with Centre for Wireless Communications (CWC), University of Oulu, Oulu, FI-90014 Finland (email: pekka.kyosti@oulu.fi) and Keysight Technologies Finland Oy, Oulu, Finland.

L. Hentilä is with Keysight Technologies Finland Oy, Oulu, Finland (e-mail: lassi.hentila@keysight.com).

Wei Fan is with the Antennas, Propagation and Radio Networking section at the Department of Electronic Systems, Faculty of Engineering and Science, Aalborg University, Denmark. Email: wfa@es.aau.dk.

J. Lehtomäki and M. Latva-aho are with Centre for Wireless Communications (CWC), University of Oulu, Oulu, FI-90014 Finland (email: firstname.lastname@oulu.fi).

tion of controllable three dimensional power angular spectrum (PAS). The overall purpose of OTA test setups is to generate fading radio channel conditions around the device under test (DUT) as specified by target channel models, like, e.g., 3GPP SCM [15], WINNER [16] or the recent 3GPP above 6 GHz model [17]. RC emulates time averaged isotropic scattering environment, but it does not provide controllable angular or polarimetric propagation characteristics, which makes it less attractive for testing of beamforming based devices. The practical capability of the reconfigurable RC is currently not fully known. RTS may in principle support also for massive MIMO, but it has two drawbacks. Firstly, it is not well suited for adaptive antenna systems like, e.g., for analog beamforming. Secondly, the required probe and fading emulator resources for the second stage are directly proportional to the number of DUT antennas. With tens or hundreds of DUT antennas the test setup may become non-feasible. Therefore, it is expected that the MPAC has the highest potential for being the OTA test method also for electrically large 5G devices.

In the literature MPAC OTA techniques for massive MIMO or mm-wave device evaluations have been discussed in [18]–[23]. In the following we summarize the work briefly. The feasibility of so called plane wave synthesis and prefaded signals synthesis methods, in terms of required number of probes, is analyzed in [18] for 2-dimensional (2D) circular probe geometries. Preliminary investigations on probe configurations and range lengths are reported in [19], with the main focus on precision of reconstructing an individual multi-path cluster. Reference [22] specifies a sectored 3D probe configuration for massive MIMO testing and presents simulation results for the minimal physical dimensions of the setup. Numerous figures of merit were used in the evaluations, from direction of arrival estimation accuracy up to multi-user MIMO sum rate capacity error. Work on the physical dimensions assessment was continued in [20], where few new metrics were used and the focus was set on 28 GHz frequency. Various aspects, like physical setup dimensions, probe configurations, and suitable channel models are discussed in [21]. Simulations were performed with 2D probe configurations only with two channel model scenarios used for 4G evaluations (SCME UMi and UMa).

Finally, [23] specifies selection criteria for the OTA method for testing of 5G equipment and discusses different alternatives. The identified criteria are: capability for real-time performance assessment, for emulating realistic radio channels, and for bidirectional (up- and downlink) emulation. They conclude that the coherent wave field synthesis is the only potential MPAC method fulfilling the criteria. We agree with [23] that with the pre-faded synthesis the reconstruction of wave fronts from arbitrary directions is not possible. However, in order to support for coherent wave field synthesis a very high number of probes and emulator resources would be required [18]. Given this, we may have to restrict the setup to capability of reconstructing wave fronts, with arbitrary fading characteristics, from the actual probe directions only. The probe requirements for wave synthesis are further discussed in section II and capabilities of the proposed system are described in section IV.

In this work we are going to introduce a complete sectored multi-probe anechoic chamber based (MPAC) over-the-air (OTA) test setup, including methods for mapping channel models onto probes. Important design parameters for the setup are its dimension, dictated mainly by the measurement distance (the range length), the configuration of switchable probes including their number and locations, and the number of active probes used for the emulation. The measurement distance has been discussed already in [20], [22]. The main contribution of the current work is to propose an upgraded MPAC method and to assess the impact of the mentioned design criteria by a set of novel simulation metrics. The focus is on mm-wave massive MIMO BS testing, but the findings are to some extent applicable also for electrically smaller devices, for lower frequencies, and for non-sectored devices (like UE).

In section II is discussed the feasibility to directly extend the conventional uniform MPAC method for electrically large devices. Section III specifies system models for the MIMO radio channel and for the corresponding OTA emulation system. Detailed description of the proposed OTA setup is given in section IV. Simulation settings and results are discussed in sections V and VI, respectively. Conclusions and a brief discussion on future work are presented in section VII.

II. Test zone size

The MPAC system is attractive for radiated testing of multi-antenna systems, due to its capability to physically emulate realistic RF environment in the anechoic chamber. Any adaptive antenna technologies (e.g. massive MIMO BS in our paper) that utilize or adapt to features of the RF environment can be therefore reliably evaluated in the MPAC setup, since it offers a realistic test condition for the device to operate normally [24]. A key question in the MPAC design to be addressed is how large a test zone size can be supported with a MPAC configuration. The test zone denotes a geometrical volume inside which target channels can be accurately reproduced.

Extensive efforts have been taken to characterize the test zone size as a function of required active OTA antennas in the literature, where two techniques are often discussed, i.e. the plane wave synthesis (PWS) and the pre-faded synthesis (PFS) technique. The objective of the PWS is to synthesize plane waves with arbitrary impinging angles within the test zone, by allocating appropriate complex weights to the active OTA antennas. Complex weights can be calculated with different techniques, e.g., the least square technique in [13], [25] or the spherical wave expansion in [26], [27]. The minimum required number of OTA antennas to synthesize an arbitrarily polarized field with an arbitrary angle can be expressed, according to the cut-off properties of the spherical wave modes [27], as

$$K_{\min} = 2\left(\lceil kr_o + n_1 \rceil\right)^2 + 4\left(\lceil kr_o + n_1 \rceil\right), \qquad (1)$$

where k is the wavenumber, r_o is the radius of the minimum sphere that encompasses the device under test, n_1 is a small integer number, and $\lceil \cdot \rceil$ is the ceil (round upwards to closest integer) operator. Typically, n_1 varies from 0 to 10 [27], [28], depending on the desired accuracy of the field synthesis. Assuming a planar DUT array with $10 \times 10 = 100$ antennas

with 0.5λ spacing, which gives the minimum r_o around 3.2λ and via setting $n_1 = 0$ and 10, we have $K_{\min} = 880$ and 1920, respectively. The minimum number of probes is very high. It was also concluded in [18], [23] that significantly more active OTA probes are needed for field synthesis in MPAC setups for massive MIMO testing object and higher frequency scenarios. Therefore, utilizing existing OTA setups as a means to test massive MIMO BSs would necessitate a substantial amount of additional hardware like probes and fading emulators, leading to cost-prohibitive designs.

With the PFS technique, the focus is on reconstructing spatial profiles in the test zone via allocating optimal power weights for probes [13]. The target continuous PAS is approximated by the discrete PAS in the PFS technique, characterized by the probe locations and probe weights. The larger the antenna aperture of the DUT, the higher beam resolution of the DUT is expected. Therefore, to ensure that the DUT can not distinguish the target and emulated spatial channel, we need more active probes to sample the PAS for DUTs with larger antenna aperture. It was concluded in [29] that using the PFS technique would yield similar estimates of the number of required probes as in the PWS technique.

Therefore, the existing MPAC configuration, i.e. with a uniform probe configuration and each probe connected to a fading emulator output port, is challenged for massive MIMO testing for mm-wave frequency bands due to cost consideration. There is a strong need to develop a new MPAC configurations that are adequate and cost-effective for mm-wave massive MIMO BS testing. Our proposed method is intended to address this need.

III. System model

In the following we define system models both for the conductive MIMO radio channel emulation and the OTA emulation.

A. Traditional MIMO emulation

The well known system model for MIMO transmission (neglecting noise) is

$$\mathbf{Y}(t,f) = \mathbf{H}'(t,f)\mathbf{X}(t,f), \tag{2}$$

where t and f denote time and frequency, $\mathbf{Y} \in \mathbb{C}^{N\times 1}$ is the received signal vector, $\mathbf{X} \in \mathbb{C}^{M\times 1}$ is the transmitted signal vector, and N, M denote the number of receiver (Rx) and transmitter (Tx) antenna ports (or sub-arrays), respectively. With a geometric channel model having L discrete paths the MIMO channel transfer function $\mathbf{H}' \in \mathbb{C}^{N\times M}$ is defined as

$$\begin{aligned}\mathbf{H}'(t,f) = \sum_{l=1}^{L} \mathbf{G}_{rx}\left(t, -\mathbf{k}_l^{rx}(t)\right) \begin{bmatrix} \alpha_l^{\theta\theta}(t,f) & \alpha_l^{\theta\phi}(t,f) \\ \alpha_l^{\phi\theta}(t,f) & \alpha_l^{\phi\phi}(t,f) \end{bmatrix} \\ \mathbf{G}_{tx}\left(t, \mathbf{k}_l^{tx}(t)\right)^T,\end{aligned} \tag{3}$$

where $\mathbf{G}_{rx} \in \mathbb{C}^{N\times 2}$ and $\mathbf{G}_{tx} \in \mathbb{C}^{M\times 2}$ are the polarimetric antenna (or sub-array) pattern vectors of θ and ϕ polarizations for Rx and Tx antenna arrays, respectively, defined to a common phase centre. Antenna patterns are introduced with argument t to support for a time variant analog beamforming. Further, wave vectors $\mathbf{k}_l^{rx}$ and $\mathbf{k}_l^{tx}$ define both the frequency and the direction of arrival/departure to sample the radiation patterns of Rx/Tx antennas, and coefficients α_l^{ab} are the complex channel gains of path l for transmitted polarization b and received polarization a. It is noted that in the formulation of eq. (3) it is assumed that all Tx and Rx antenna elements experience the same propagation coefficients α. This assumption is not valid if the far field condition does not hold. To model these cases the propagation coefficients have to be defined separately for Tx/Rx element pair, as is done, e.g., in [30].

In traditional conducted MIMO emulation UE antenna ports and DUT (BS) antenna ports are connected to fading emulator input/output ports with coaxial cables. Within the fading emulator the input signal $\mathbf{X}$ is multiplied (convolved in time domain) with the channel matrix $\mathbf{H}'$ and the signal vector $\mathbf{Y}$ is fed to N ports of the DUT.

For terminology, from now on the uplink transmission is assumed, i.e. DUT (BS) is the receiver and the transmitter is UE or UE emulator. Though, the emulation can be also to downlink direction or bi-directional, where the latter one is expected as the most typical test mode.

B. OTA emulation

In OTA case the transfer function $\mathbf{H}'$ is composed by operations of the fading emulator and the MPAC setup illustrated in Fig. 1. In eq. (2) $\mathbf{H}'$ is substituted by

$$\mathbf{H}(t,f) = \mathbf{F}(t,f)\mathbf{W}(t,f). \tag{4}$$

The transfer matrix from K OTA probes to N DUT antennas is

$$\mathbf{F}(t,f) = \{\gamma_{n,k}(t,f)\} \in \mathbb{C}^{N\times K}, \tag{5}$$

with entries

$$\begin{aligned}\gamma_{n,k}(t,f) =& \mathbf{G}_{rx,n}\left(t, -\mathbf{k}_{n,k}\right) \mathbf{G}_o\left(\mathbf{k}_{n,k}\right)^T \\ & \sqrt{L(d_{n,k},f)} e^{j\|\mathbf{k}_{\mathbf{n},\mathbf{k}}\| d_{n,k}},\end{aligned} \tag{6}$$

where $\mathbf{G}_{rx,n}$ and $\mathbf{G}_{o,k} \in \mathbb{C}^{1\times 2}$ are the polarimetric antenna pattern vectors of nth DUT antenna and kth OTA probe, respectively. Further, $\mathbf{k}_{n,k}$, $d_{n,k}$ and $L(d_{n,k})$ are the wave vector, the distance and the path loss term between the kth probe and the nth DUT antenna, respectively. It is noted that the time dependency of $\mathbf{F}$ results only from possible time variant analog weighting of DUT antennas. Otherwise the transfer matrix is static.

The transfer matrix $\mathbf{W} \in \mathbb{C}^{K\times M}$, containing predominantly the temporal and the frequency fading components of the channel model, is defined as

$$\begin{aligned}\mathbf{W}(t,f) = \sum_{l=1}^{L} \mathrm{diag}\left(\mathbf{\Gamma}_l(t)\right) \mathbf{G}_{id} \\ \begin{bmatrix} \alpha_l^{\theta\theta}(t,f) & \alpha_l^{\theta\phi}(t,f) \\ \alpha_l^{\phi\theta}(t,f) & \alpha_l^{\phi\phi}(t,f) \end{bmatrix} \mathbf{G}_{tx}^T\left(t, \mathbf{k}_l^{tx}(t)\right),\end{aligned} \tag{7}$$

where $\mathbf{G}_{id}$ is $K \times 2$ ideal polarimetric antenna pattern matrix of OTA probes with entries $\in \{0, 1\}$ and the vector $\mathbf{\Gamma}_l(t) = \{g_{l,k}(t)\}$, $k = 1, \ldots, K$, is composed of weights of K probes for the lth cluster. In principle it is possible to set the weights also frequency dependent in the fading emulator by substituting each scalar $g_{l,k}$, e.g., by a linear filter. However, we expect this is not necessary on the considered fractional bandwidths (BW) like, e.g., 0.8 GHz BW at 28 GHz or 2 GHz BW at 60 GHz.

Ideally the target in faded OTA emulation would be to reach condition $\mathbf{H}' = \mathbf{H}$. On the conceptual level this could be achieved simply by determining $\mathbf{F}$ and specifying

$$\mathbf{W}(t, f) = \mathbf{F}(t, f)^{-1}\mathbf{H}'(t, f). \tag{8}$$

However, this cannot be carried out in practice. The OTA transfer matrix $\mathbf{F}(t, f)$ is not typically measurable (or otherwise determinable), neither over frequency because the DUT may not support for measuring the S_{21} parameter, nor over time because the dynamic beam allocation of a DUT is not known a priori.

Instead of the aforementioned, i.e. using eq. (8), we choose active probes properly and control weights $g_{l,k}(t)$ to reach statistically similar transfer functions $\mathbf{H}'$ and $\mathbf{H}$ of the reference and the OTA case, respectively. Methods for the probe selection and the weight determination are discussed in detail in sections IV-B and IV-C, respectively. By statistically similar we mean, e.g., same power delay profile, Doppler spectrum, Ricean K-factor, amplitude distribution, cross polarization power ratio, and power angular distribution, as with the target channel model. With the popular geometry based stochastic channel models [15]–[17] the instantaneous channel coefficients are not specified, thus it is not feasible to pursue for any particular instantaneous fading channel conditions.

As described in [13] the time and frequency variation of the radio channel is mostly reconstructed within the fading emulator and these dimensions do not require any special treatment compared to the state-of-the-art conductive emulation. The challenging part is to reconstruct the polarimetric and especially the spatial field within the test zone. Procedures for this are proposed in the next section.

IV. MPAC OTA FOR MASSIVE MIMO DEVICES

The current MPAC setup for LTE UE is composed of an anechoic chamber containing a number of probes (also called OTA antennas) typically in a 2D ring formation, a fading emulator, and a communication tester. The DUT is located in the centre of the probe ring, which most commonly contains eight dual polarized probes with 45° azimuthal spacing. The intention is to synthesise time variant controllable electromagnetic (EM) field within a cylindrical test volume. Either PFS or PWS can be used to reconstruct the EM fields [13] following the statistical propagation characteristics specified by a target channel model.

There are a number of differences between LTE UEs and the coming mm-wave massive MIMO BSs in terms of devices and typical propagation parameters, as listed in [21], [22]. While UEs are normally designed for isotropic reception and used close to scatterers, BSs are typically installed on a wall or similar to serve a sector of angles. So, BSs are located higher and farther from scatterers compared with UEs. Thus the angular power distribution of BSs is expected to be confined in the angle region, be more specular, and require definitely emulation of 3D propagation. The last remark follows also from the vertical beamforming capability of BSs. In the current standard LTE UE test systems [9], [10] the 2D probe configuration and field synthesis is seen sufficient.

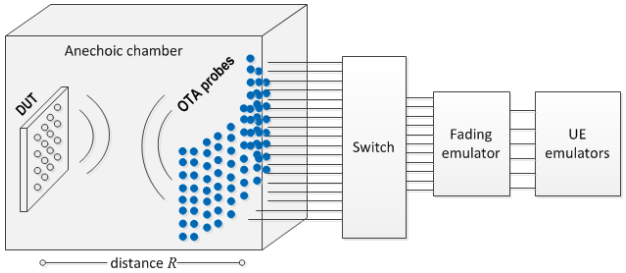

Fig. 1. Components of the sectored MPAC OTA setup.

Components of the proposed setup are illustrated in Fig. 1. Anechoic chamber serves mainly for shielding from external signal sources, but also for preventing unwanted reflections. In Fig. 1 the test zone is located in one end of the chamber and DUT placed in the centre of the test zone, which is also the origin of the coordinate system, as shown in Fig. 2. A large number of probes is located on a sector of angles with approximately equal distance R from the origin and with certain angular spacing. In principle the variation of R across probes can be compensated by phase and amplitude calibration. In practice achieving phase coherence may be difficult in any case. For example the switch implementation and the long term phase drift effects related to the ambient temperature are concrete challenges.

Probes for 28 GHz can be fabricated on printed circuit board. They are cheap to manufacture and the major constraint on the number of them comes from the space. A number of probes can be placed on a single board with certain size, these boards are called probe panels from now on. While probes may be cheap the fading emulator resources and possibly required analog components, like power amplifiers and up/down converters, are not. Thus only a sub-set of probes are switched to the fading emulator by a real-time controllable switch. The switching and the selection of the probe sub-set, is based on the target channel model for optimizing the usage of fading emulator resources. Fading emulator has RF input and output ports. It performs the channel modulation operation specified in eq. (2) with the definable transfer matrix $\mathbf{W}$ from eq. (4). UE emulator imitates the other link end. In practice it can be replaced by a real UE or a number of UEs (emulators). If only up- or downlink is in the focus of fading emulation, the other link direction can be communicated with a dedicated probe antenna and a cable connection bypassing the fading emulator. This approach is similar to the current LTE OTA configurations [10].

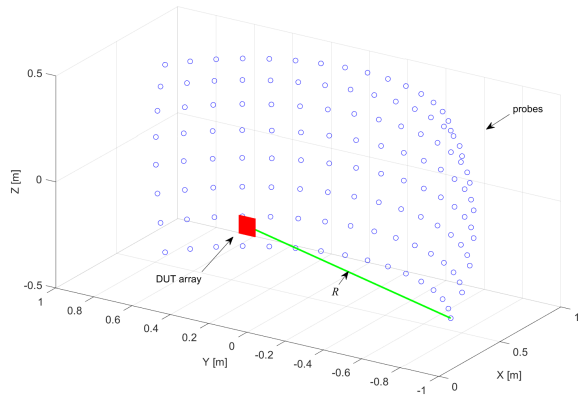

Fig. 2. An illustration of the sectored probe configuration.

A. Mechanical rotation of DUT

In the case of sectored probe configuration the probe panels are covering only a limited sector of angles. With BS devices the broad side of DUT array is known. In order to utilize the angular sector covered by probes the DUT is first rotated mechanically with respect to the probe panels based on a priori information of the channel model. For example the probe panels may be located to an elevation sector of $+30° \cdots -30°$ and the strongest propagation paths in the channel model to be emulated may be specified to below $-30°$. In this case it is beneficial to rotate the DUT such that directions of main paths fit the probe panels. Alternatively, the DUT may be attached to a fixture with a specifiable rotation angle. Thus the first step of establishing an OTA emulation is to calculate, e.g., a centre of gravity of the model PAS and to rotate the DUT such that maximal amount of PAS coincides with the probe sector. Optionally the rotation may be performed such that the strongest path angle turns to the probe closest to the positive x axis direction in the coordinate system specified in Fig. 2.

B. Probe allocation

The next step is to choose a sub-set of probes from the full set available in the setup. Typically the sub-set size is determined by the available fading emulator resources. Allocation of probes is performed by connecting the selected ones to fading emulator ports with the switch illustrated in Fig. 1. In a practical setup the switch implementation may also restrict the degrees of freedom of probe allocation. For example it may not be feasible to implement a switching matric from all probes to all fading emulator ports. However, in the simulation section of this work a full freedom is assumed.

Here we propose an algorithm for selecting at maximum K probes from the full set for emulating a channel model with known cluster nominal angles β_l, i.e. angles of $-\mathbf{k}_l^{rx}$, and cluster powers P_l. Assume that the DUT is rotated as defined in IV-A. Now K probes are allocated as follows. Sort cluster powers P_l to descending order. Allocate the closest probe to each angle β_l until K probes are allocated. However, do not allocate a probe to a cluster if the angular distance between β_l and the probe direction is above a threshold, say e.g. $10°$. This is mainly to prevent allocating probes to clusters outside the probe panels. If less than K probes is allocated at this point a second round is started. Now again take power sorted clusters and allocate as many probes as possible around the strongest cluster within limit of the mentioned threshold. Repeat the procedure with weaker clusters until K probes are selected. Fig. 3 shows an example of probe allocation.

Other, more complex and sophisticated, allocation algorithms can be developed. For this purpose different criteria and cost functions can be defined. The optimization can be based, e.g., on minimizing a spatial correlation function error or a reconstructed PAS error. The above described method is simple, but still rather competent, at least when the per-cluster angular spreads of the emulated channel model are not large.

The defined probe allocation is based on angular characteristics of the propagation channel. Some clusters may stay without dedicated probes, if, e.g., the probe panels do not cover wide enough angular sector of if K is less than the number of clusters. In this case also these remaining clusters are mapped to the selected probes, as described in the following subsection. This conserves the power delay profile (PDP) of the propagation channel, but may distort the PAS and the joint power angular delay profile, if the probe allocation is not sufficient.

C. Probe weighting

The next task is to find weights $g_{l,k}$ of eq. (7) for the allocated probes. A straightforward method would be to sample the known model PAS with the known probe locations. Here is assumed that the reference channel model specifies for each cluster l a continuous PAS $P_l(\Omega)$ for space angles Ω, that can be sampled by probe directions. This is the case with most geometry based stochastic channel models, where typically clusters have 2D Laplacian function shaped PAS with specific spread parameters. Now the direct sampling is simply

$$g_{l,k}^2 = \frac{P_l(\xi_k)}{\sum_l \oint P_l(\Omega) d\Omega}, \tag{9}$$

where ξ_k is the space angle of the kth probe (angle of wave vector $\mathbf{k}_{0,k}$ from probe k to the origin). However, this procedure does not consider the limited aperture of DUT and does not lead to optimal weighting.

Another weighting method, aiming to minimize the spatial correlation error, is defined in [13] in context of PFS method. There a cost function is composed of the spatial correlation function of the reference model and the allocated probe configuration within volume of the test zone. The spatial correlation function is Fourier transform pair with PAS $P(\Omega)$ and carries the same information with it. For any pair of spatial locations $q = (\mathbf{p}_{q1}, \mathbf{p}_{q2})$ defined by location vectors $\mathbf{p}$, the spatial correlation can be written as

$$\rho_q = \oint P(\Omega) \exp\left(j\boldsymbol{\Omega} \cdot (\mathbf{p}_{q1} - \mathbf{p}_{q2})\right) d\Omega, \tag{10}$$

where $\boldsymbol{\Omega}$ is the wave vector from space angle Ω. The spatial correlation function achievable with an MPAC setup, considering the number, directions, and distances of probes, can be calculated according to [21] as

$$\hat{\rho}_q = \frac{\sum_{k=1}^{K} g_k^2 L(d_{p1,k}) L(d_{p2,k}) \exp\left(j\|\mathbf{\Omega}\|(d_{p1,k} - d_{p2,k})\right)}{\sqrt{\sum_{k=1}^{K} L^2(d_{p1,k}) g_k^2 \sum_{k=1}^{K} L^2(d_{p2,k}) g_k^2}}, \tag{11}$$

where K is the number of probes, g_k is the amplitude weight of the kth probe, $d_{p1,k}$ and $L(d_{p1,k})$ are the distance and the path loss term between the kth probe and the location $\mathbf{p}_{q1}$, respectively. Now for each cluster l is searched the set of weights $g_{l,k}$ that minimizes the cost function

$$\mathbf{\Gamma}_l = \arg\min \sum_{q=1}^{Q} \left|\rho_q - \hat{\rho}_q\right|^2, \tag{12}$$

where Q is the number of location pairs. Finally each weight vector $\mathbf{\Gamma}_l$ is normalized to unity gain. This method was selected for the simulation part of this work. Alternatively the cost function can be composed, e.g., to minimize the deviation of the reference PAS and the PAS constructed by the OTA setup, both as observed by a limited aperture of the DUT.

It is important to notice that in a practical system the weights $g_{l,k}$ may contain also phase and amplitude compensation for impairments on signal paths, probe gains, etc. The compensation coefficients can be determined by a calibration procedure performed in an initial step with, e.g., a network analyzer and a known calibration antenna placed within the test zone. Beneficially, with PFS the phase accuracy between probes is not mandatory as stated in [31]. However, the phase coherence is required between co-located orthogonally polarized probe elements, even with PFS, if target is to control polarization states.

The steps described above can be extended to multi-UE case. There the rotation and probe allocation is optimized for the joint PAS of all UEs, while probe weighting procedure is repeated for each UE separately, but keeping the relative powers of UE clusters balanced. Of course, resources in terms of channel emulators (active ports and logic channels), RF splitters and combiners, and the required angle region might be increased.

D. Probe panel design

In this work we discuss and evaluate mainly the reconstruction of spatial/angular characteristics of radio channel models for OTA emulations. These aspects affect the design of arrays of probes on probe panels. Especially the range length, the covered sector of angles, the angular spacing of probes, and the number of selectable probes. The first three design criteria, together with possible manufacturing constraints, determine the dimensions of probe panels and the locations of probes within panels.

Another radio channel dimension to be covered is the polarization. Each probe antenna must support for transmission/reception of controlled polarization state. This can be achieved similarly to the existing LTE MPAC OTA setups, by utilising co-located orthogonally polarized probe elements. Both polarizations have separate feed and the phase difference between elements must be able to be compensated out after a calibration measurement. The polarization control is important, especially if the spatial multiplexing in the coming pre-5G systems will be performed utilizing orthogonal polarization.

In some 5G performance measurements the OTA emulation of both uplink and downlink fading may be crucial. This requirement affects the probe panel design, particularly when the full reciprocity of uplink and downlink fading channels is aimed at. In the present study we assume ideal conditions and do not specify whether the probes are in receiving or transmitting mode.

An interesting topic for a future work is to investigate reflections from probe panels, as they may contribute distortion to the reconstructed PAS. In [32] a compensation at 1.5 GHz setup was performed. However, in the present work we assume ideal chamber conditions.

V. Simulation Settings

The simulation system follows the description of section IV. Purpose of the simulations is to evaluate the performance of MPAC OTA setup with different probe configurations and other parameters, utilizing metrics described in section VI-A.

A. Simulation parameters

The parameters varied in simulations are listed in Table I. The range length R was between 1 and 10 metres, where the simulated 4 and 10m range lengths would be very challenging for a practical setup due to link budget issues. Here they are considered mainly for comparison. The maximum number of probes selected for reconstruction of the angular power distribution was between 4 and 16. In all cases the panels of probe antennas covered 120° in azumuth angles and in elevation either 30° or 60°. The angular spacing of probes in panels was either 7.5° or 3.75°.

In total seven channel models were simulated. They are all 3GPP clustered delay line (CDL) models specified in [17], without any scaling in angular or delay domains. The first three models $M1-M3$ are for non-line-of-sight (NLOS) condition as shown in Table I, while the last four $M4-M7$ are for line-of-sight (LOS) condition. Ricean K-factor of $M4$ and $M6$ is 3 dB and with $M5$ and $M7$ it is 9 dB. In all models the LOS direction of the UE was in AoD $= 31°$ and EoD $= -31°$ and the NLOS path directions orientate according to it. We do not expect the CDL models of [17] to be the best possible or the most representative models for 5G radio links, but they were chosen to have a clear and well defined reference.

Finally, four different DUT array configurations were taken as specified in Table II. In all cases the DUT has uniform rectangular array with half wavelength spacing between elements. DUTs $D1$ and $D2$ have 64 vertically polarized elements. Array $D1$ is located in the centre of the test zone (origin of the coordinate system), while $D2$ is displaced by 2.1 cm to directions of the positive y and z axes. DUTs $D3$ and $D4$ are analogous, but with in total 256 elements and displacement of 4.3 cm. The displacement offset is chosen to imitate cases where the DUT may have several sub-arrays off from to DUT centre, e.g., sub-arrays with different orthogonal polarizations are possibly not co-located. The offset should

TABLE I
LIST OF VARIED PARAMETERS IN SIMULATIONS.

Parameter	Values and unit
Range length R	1, 2, 4, 10 m
Max num. of active probes	4, 8, 12, 16
Elev. range of probe panels	30°, 60°
Angular spacing of probes	7.5°, 3.75°
Channel model	$M1$, $M2$, $M3$, $M4$, $M5$, $M6$, $M7$ (NLOS A, B, C, LOS D3, D9, E3, E9)
DUT arrays	$D1$, $D2$, $D3$, $D4$

TABLE II
SIMULATED DUT ARRAYS.

	DUT	dimensions width × height × diag. [cm]	offset [cm]
$D1$	8×8	$4.3 \times 4.3 \times 6.1$	$y = 0, z = 0$
$D2$	8×8	$4.3 \times 4.3 \times 6.1$	$y = 2.1, z = 2.1$
$D3$	16×16	$8.6 \times 8.6 \times 12.1$	$y = 0, z = 0$
$D4$	16×16	$8.6 \times 8.6 \times 12.1$	$y = 4.3, z = 4.3$

reduce the emulation accuracy only in the cases where the far field criterion is not fulfilled.

B. Simulation procedure

The procedure of evaluating different setup configurations is as follows. As the first step 1000 time samples of the ideal reference channel transfer matrices of eq. (3) were generated with Keysight Geometric Channel Modelling Tool^{TM} for different model and DUT combinations. Secondly the transfer matrices of eq. (4) for OTA setups were generated in a Matlab^{TM} simulation environment for all parameter combinations of Table I. As intermediate operations of the second step the probe allocation and weighting was performed according to the description of section IV. Probes are assumed isotropic vertically polarized elements. In practice it is a requirement that the probe elements have sufficient flat radiation pattern to the direction of the test zone. Finally different metrics were calculated comparing the reference and OTA cases as described in the following section.

In the simulations was assumed isotropic radiation pattern $\mathbf{G}_{tx}$ for the Tx (UE) antenna. Thus the UE illuminated all clusters present in the channel model. The resulting PAS for the Rx (DUT/BS) would have been more confined if also the UE side performed beamforming. Currently the operational mode of the other link end, e.g. UE emulator in this case, in the coming OTA performance evaluations is not defined. In other words, it is not specified whether the other link end should operate in close to isotropic mode, or in beamforming mode with a single static beam, or in its normal adaptive beamforming mode. These alternatives are expected to set different requirements for the probe configurations. The first option would require many probes spread to directions of all clusters. In the second option probably only one or few clusters are illuminated and less active probes are needed in a confined sector of angles. In the third option only one or few clusters are illuminated simultaneously, but the illuminated clusters may change over time according to active beam states. In this case the switching capability, used to change the active probes dynamically, might be very useful to save fading emulator resources.

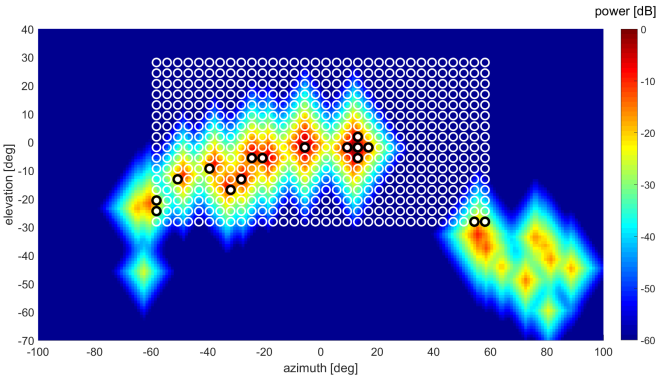

Fig. 3. Reference PAS of model $M3$ and the corresponding probe selection (in the coordinate system of probes).

Figure 3 illustrates the theoretical PAS of model $M3$ (NLOS C). In the figure is also shown the available probes with white circles in the case of 60° elevation range and 3.75° probe spacing. The selected probes, at maximum 16 in this example case, are denoted with black circles. Notice that in the example figure the PAS is rotated to the broad side of DUT, i.e. the polar coordinate system in the figure is that of the probe sector, not of the DUT.

VI. SIMULATION METRICS AND RESULTS

A. Evaluation metrics

1) Total variation distance of PAS: The purpose of this and the next metric is to evaluate how well the OTA setup is capable of reconstructing a target PAS. The metrics should reflect both the PAS itself and also the DUT size and resolution. The total variation distance of power angular spectra is defined as follows. First the PAS is estimated utilizing the classical Bartlett beamformer [33] with the assumed DUT array. This corresponds to filtering the actual power angular distribution of the propagation channel by the limited aperture of the DUT array. The PAS estimate is calculated for the ideal reference model as

$$\hat{P}_r(\Omega) = \mathbf{a}^H(\Omega) \left(\oint \mathbf{a}(\Omega') P(\Omega') \mathbf{a}^H(\Omega') d\Omega' \right) \mathbf{a}(\Omega) \quad (13)$$

and the discrete implementation of the reference model by the OTA setup as

$$\hat{P}_o(\Omega) = \mathbf{a}^H(\Omega) \mathbf{R}_o \mathbf{a}(\Omega), \quad (14)$$

where $\mathbf{a}(\Omega)$ is the array steering vector of DUT array to the space angle Ω and $P(\Omega')$ is the PAS of the reference channel model. Further, $\mathbf{R}_o = \{\hat{\rho}_q\}$ is the correlation matrix which entries are the spatial correlation coefficients between DUT element locations specified in eq. (11). An example of $\hat{P}_r(\Omega)$ estimated with DUT $D1$ is shown in Fig. 4.

Next, both estimated spectra are normalized to sum power of unity such that they can be interpreted as 2D probability

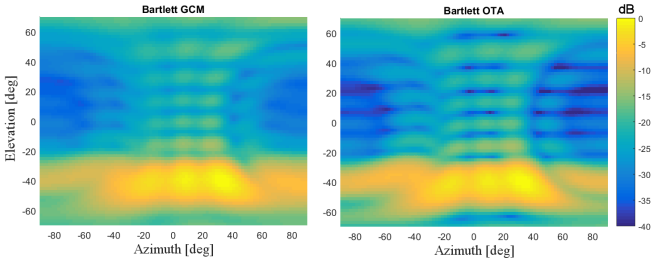

Fig. 4. PAS of model $M3$ (in the coordinate system of DUT) estimated by Bartlett beamforming with DUT $D1$ in the reference case (left) and OTA case (right).

distribution functions. Finally the total variation distance between the normalized PAS is calculated

$$D_p = \frac{1}{2}\int \left| \frac{\hat{P}_r(\beta)}{\int \hat{P}_r(\beta')d\beta'} - \frac{\hat{P}_o(\beta)}{\int \hat{P}_o(\beta')d\beta'} \right| d\beta. \tag{15}$$

The range of D_p is $[0, 1]$, where zero denotes full similarity and one maximal dissimilarity, respectively.

2) Spatial correlation error: The intention of the test system is to reconstruct the PAS of the original channel model as accurately as possible. We need a metric to evaluate how well the reconstruction succeeds. Comparing a continuous target PAS to the inevitably discrete PAS achievable by a limited number of probes is problematic [13]. With this metric we aim to evaluate the spectra indirectly via the spatial correlation function.

The idea is to assess the spatial correlation error on a particular test zone within the setup. The error indicates deviation of the ideal target PAS and the PAS achievable with an MPAC setup, specified in eq. (10) and (11), respectively. The weighted RMS correlation error is defined as

$$e_\rho = \sqrt{\frac{1}{Q}\sum_{q=1}^{Q} |\rho_q - \hat{\rho}_q|^2 \max\left(|\rho_q|, |\hat{\rho}_q|\right)}. \tag{16}$$

Weighting by the corresponding correlation level is performed to emphasize the significance of the deviation. Namely, even small deviation on the magnitude of correlation coefficient when it should be close to unity has impact on, e.g. the spatial multiplexing performance, while possibly larger deviations at low correlation levels are less significant.

3) Beam peak distance: The motivation of beam selection metrics, this and the next one, is the assumption that the DUT is utilizing fixed beams having a discrete code book of antenna weights. We assume the DUT array can at least partly perform analog combining of elements (analog beamforming) to compose beams to a pre-defined set of directions. This mode of operation is expected with devices in so called pre-5G systems [4]. It is further assumed the DUT array is well calibrated and the fixed main beams are targeted to a certain grid of directions. Like, e.g., in Fig. 5 the grid has 56 directions, four in elevation and 14 in azimuth. In the figure and in the beam selection metrics is assumed that the beam with highest power is selected per time instant among the all fixed beam. The

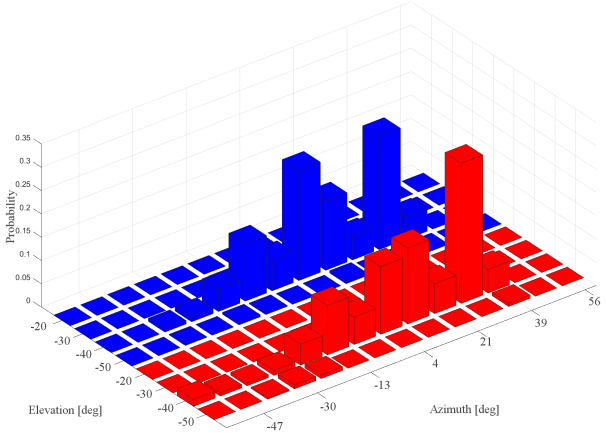

Fig. 5. Fixed beam directions and their probabilities with the reference model $M3$ (blue) and in the OTA case (red).

strongest beam is found by sequential scanning of all beam powers. Fig. 5 shows probabilities of certain beam found as the strongest. The DUT in simulations for the figure was $D1$ and the other settings were as described with the Fig. 3. In NLOS models the temporal variation, i.e. fading, of propagation paths spreads the probability distribution. In LOS models, especially with high Ricean K-factor, typically the beam of LOS direction carries constantly the highest power and the distribution is a single peak.

It is worth of noticing that comparing instantaneous beam selection between the reference and the OTA case is not possible in the simulations. However, this should not be interesting either, because typical channel models are essentially describing statistical characteristics of propagation channels and the instantaneous channel realizations are not specified.

Beam peak distance is the angular distance between probability weighted average directions of the allocated beams with the unit of degrees,

$$D_b = \left\| \sum_{b=1}^{B} \Omega_b p_r(\Omega_b) - \Omega_b p_o(\Omega_b) \right\| \tag{17}$$

where B is the number of fixed beams i.e. the pre-allocation code book size of the DUT, $\Omega_b = (\phi_b, \theta_b)$ is the azimuth and elevation angle of the bth beam, p_r and p_o are probabilities of the beam allocation on the reference and the OTA case, respectively.

4) Total variation distance of beam allocation distributions: is another beam selection metric. Here the total variation distance is calculated for 2D beam allocation distributions as

$$D_s = \frac{1}{2}\sum_{b=1}^{B} |p_r(\Omega_b) - p_o(\Omega_b)| \tag{18}$$

Similarly to eq. (15) D_s has values in range $[0, 1]$, with the same interpretation.

5) Fixed beam power loss: In addition to the four general metrics, we use the fixed beam power loss to evaluate the range length only. The metric assumes a communication system with fixed beams, i.e. with a discrete code book of DUT antenna

weights. The purpose is to determine how much power is lost in average, due to curvature of wavefronts at the test zone. The power loss for a wave from direction of nth probe is Q_n and the average power loss Q_{av} is the mean over all n. The metric is defined in [20] and we leave the detailed description to be found there.

B. Simulation results

The mentioned four metrics were determined from simulations with the parameters defined in Table I. The number of parameter combinations, i.e. simulation cases, is high, in total 1792. Due to space limitation it is not possible to show the results for this high number of cases. Instead of trying to visualize the six dimensional data set we present the results as follows. We observe the trends and typical behaviour from the whole data set and describe the findings in this section. For visualization of the impact of a certain configuration parameter we fix the other variables, except DUT types, and choose one example figure for a NLOS model and one for a LOS model. The fixed configuration parameter values are: range length 2 m, eight active probes, elevation sector $60°$, and the angular probe spacing in panels $7.5°$.

Finally we show the simulated metrics for combinations of DUTs and channel models, with all configuration parameters fixed to the recommended values. In each of the Fig. 7–15 the four bar diagrams are as follows: top left is the Total variation distance of PAS, top right is the Spatial correlation error, bottom left is the Beam peak distance, and bottom right is the Total variation distance of beam allocation distributions.

1) Range length: Fig. 7 and 8 show the impact of range length R on the four metrics with NLOS model $M3$ and LOS model $M7$, respectively. With the NLOS model R does not affect the PAS based metrics (Total variation distance of PAS and Spatial correlation). It has a small impact on the beam selection metrics with $D2$ and $D4$, i.e. with the DUTs off from the test zone centre. Similarly the DUTs with location offset gain from larger R with the LOS model, but in LOS this is observable also on the Total variation distance of PAS metric.

We can conclude that for $D1$ and $D3$, i.e. for DUT arrays up to 16×16 without offset, the range length of $R = 1$ m is sufficient with all simulated channel models. OTA emulation of DUT $D2$ would give slightly higher precision if $R > 1$ m. Distinctly $D4$, representing a very large DUT, would require $R = 2$ m or higher.

Similar conclusions can be drawn from the fixed beam power loss simulations of Fig. 6 (left). There DUTs $D1 - D3$ have acceptable $Q_{av} < 2$ dB with $R = 1$ m, which was chosen as the threshold of the average fixed beam power loss in [20]. $D4$ has above 2 dB loss even with $R = 2$ m. Further, we can observe that with this metric $R = 0.5$ m may be too short for $D2 - D4$. The maximum fixed beam power losses, among all directions of the probe sector, are illustrated in Fig. 6 (right). Even these are below 1 dB with $D1 - D3$ and $R = 1$ m.

2) Number of active probes: The diagrams of Fig. 9 and 10 illustrate how the number of probes that can be simultaneously switched to the fading emulator affects the metrics with NLOS model $M3$ and LOS model $M5$, respectively. In the LOS case there is practically no performance difference with different probe numbers. This follows mainly from the dominant role of the LOS path. The other paths have such an insignificant contribution that adding more probes does not perform considerably better. With NLOS models, however, the increased probe number has a positive impact. The PAS based metrics indicate remarkable improvement when taking eight probes instead of four. The beam selection metrics do not show a clear trend. There, in some cases the more probes results to worse accuracy. The beam peak distance, being based on the centre of gravity of 2D probability histograms, is quite sensitive even to small changes of reconstructed discrete PAS, when the model has many close to equal strong clusters (see Fig. 5). This may explain the unstable behaviour of that metric in the simulated case.

Four simultaneously active probes is a sufficient number for LOS channel models. With NLOS models the adequate number with all DUT types is eight. Though, some accuracy gain is achievable utilizing even 12 or 16 simultaneous probes. It is important to remember that this configuration parameter is heavily dependent on the channel model to be emulated. If the target PAS is highly spread, i.e. it has high azimuth and elevation angular spreads, and possibly has numerous equal strong directions, then many active probes are required.

3) Elevation sector covered by probes: The elevation coverage by probe panels is investigated in Fig. 11 and 12 for the NLOS model $M3$ and the LOS model $M6$, respectively. Similarly to the probe numbers, the LOS model is insensitive to the elevation coverage. Also the reason is same, i.e. the strong centralization of PAS to the LOS path. In the selected NLOS model there is a slight performance enhancement with $60°$ elevation sector, except with the metric of Total variation distance of beam allocation distributions.

This is another setup configuration parameter that is strongly dependent on the channel model, in particular the target PAS. In 3GPP model [17] the composite elevation spreads are rather narrow and the power may be confined to a $30°$ elevation sector. The $30°$ elevation sector can be considered sufficient for the single UE emulations. However, when emulating multiple users, e.g., MU-MIMO systems, the need for elevation coverage of probe panels may easily increase to $60°$.

4) Angular spacing of probes within panels: Impact of the spacing of selectable probes with the NLOS model $M3$ and the LOS model $M4$ is depicted in Fig. 13 and 14, respectively. With NLOS models the total variation distances show some gain with increased angular resolution by probe panels. The spatial correlation error has no difference on smaller DUTs $D1$ and $D2$, but has clear improvement with the two larger DUTs. Again the beam peak distance is somewhat unstable while the results indicates opposite trend. With LOS models there is no remarkable difference between $7.5°$ and $3.75°$ resolutions.

At least with 8×8 DUT arrays the $7.5°$ spacing of selectable probes is adequate. The larger DUTs with NLOS models benefit from denser spacing, but the gain is not necessarily significant.

5) General remarks: As a general observation from simulation results we can remark that LOS channel models are more

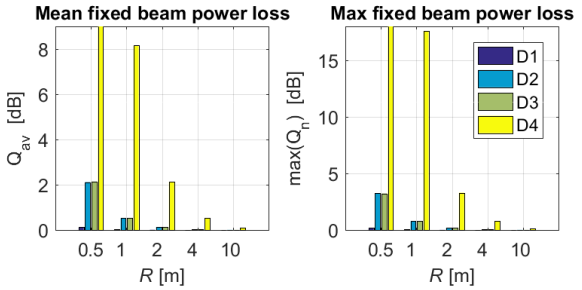

Fig. 6. Impact of range length on the metric average (left) and maximum (right) fixed beam power loss.

sensitive to the range length while NLOS models are more sensitive to the other probe setup configuration parameters. This is a consequence of the dispersion of power in angular domain. In LOS models the PAS is typically more impulse like and in NLOS models there is a wider spread. In principle the more dispersed the PAS is the more probes are needed, which is a very intuitive conclusion too.

Based on the findings the recommended configuration parameters for DUTs sized up to 16×16 without displacement, i.e. $D1$–$D3$, are as follows: range length $R = 1$ m, eight simultaneously active probes, $30°$ elevation sector covered by probe panels, and with $7.5°$ angular spacing of probes. The range length of 1 m is supported also by simulations of [20]. There a metric called *Fixed beam power loss* was used for a 20×20 planar array and the minimum $R = 1$ m was concluded. The metric assumes DUT array using a code book of fixed beams and it indicates the amount of lost power due to curvature of the received wave fronts. The overall recommended configuration aims to save in the cost and size of the test setup while still keeping the accuracy on an appropriate level.

Performance of all DUT and channel model combinations with the recommended parameter set is shown in Fig. 15. We can observe that LOS models can be reconstructed with higher precision in all cases than the NLOS models. The only exception to this is the total variation distance of PAS with DUT $D4$. As discussed earlier $D4$ suffers from short range lengths in LOS cases. Further, model $M1$ shows the worst performance when measured by the PAS based metrics. This follows from the PAS shape of $M1$ whose elevation spread is more than ten-fold compared to the other models. It has one strong cluster and the other clusters are very widely spread outside the probe panels both in azimuth and elevation. The other clusters are such weak, on the other hand, that beams are never allocated to them and thus the beam selection metrics perform decently. Moreover, model $M2$ has highest inaccuracies with the beam selection metrics. In $M2$ the PAS is composed of several close to equal strong clusters and in the reference case more than 20 different beams get allocated. Reconstruction of this condition with limited probe resources in the anechoic chamber is evidently difficult.

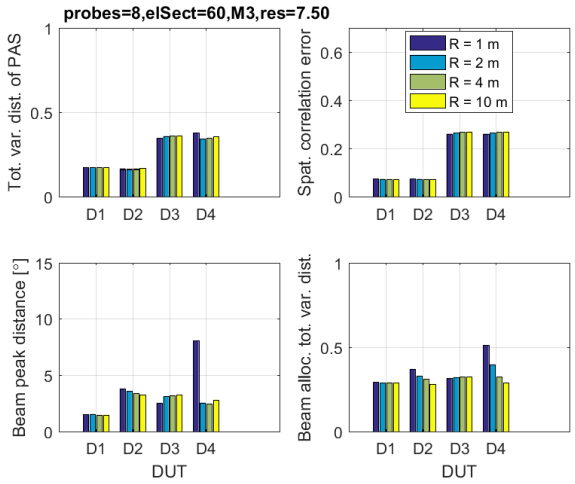

Fig. 7. Impact of range length on performance metrics, NLOS $M3$.

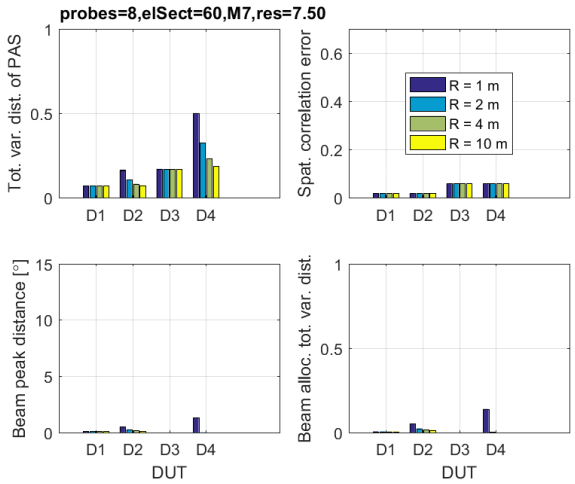

Fig. 8. Impact of range length on performance metrics, LOS $M7$.

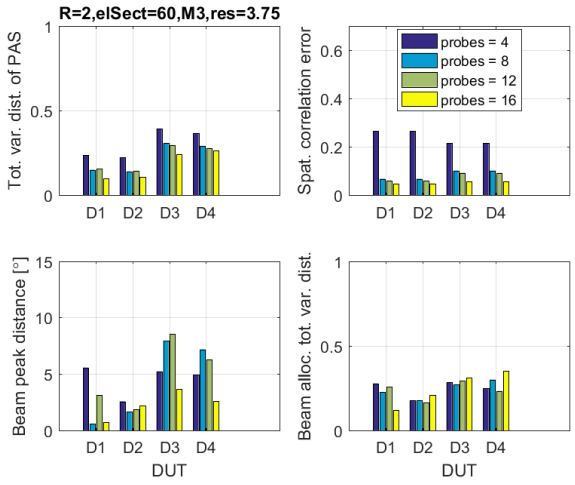

Fig. 9. Impact of active probe number on performance metrics, NLOS $M3$.

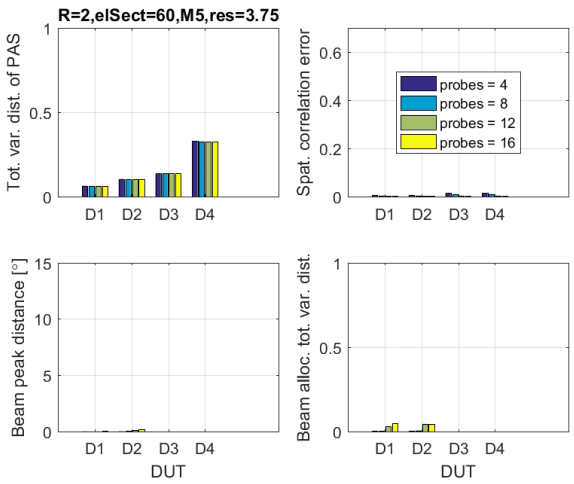

Fig. 10. Impact of active probe number on performance metrics, LOS $M5$.

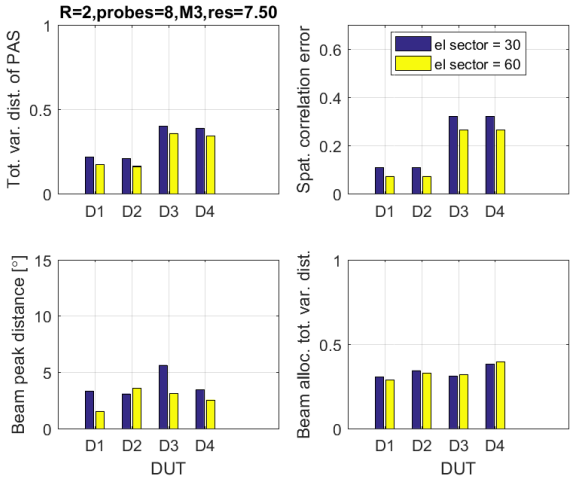

Fig. 11. Impact of elevation sector on performance metrics, NLOS $M3$.

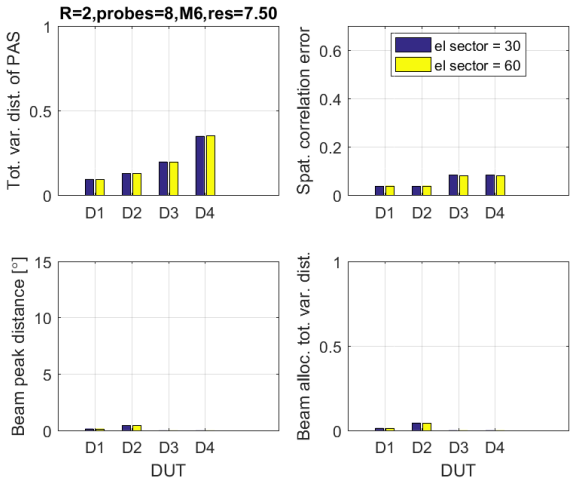

Fig. 12. Impact of elevation sector on performance metrics, LOS $M6$.

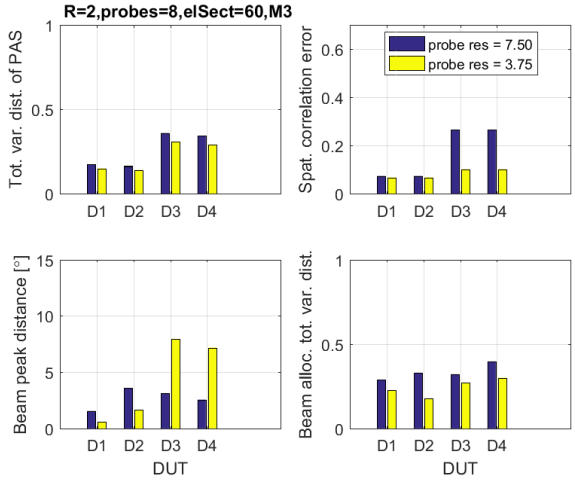

Fig. 13. Impact of probes angular spacing on performance metrics, NLOS $M3$.

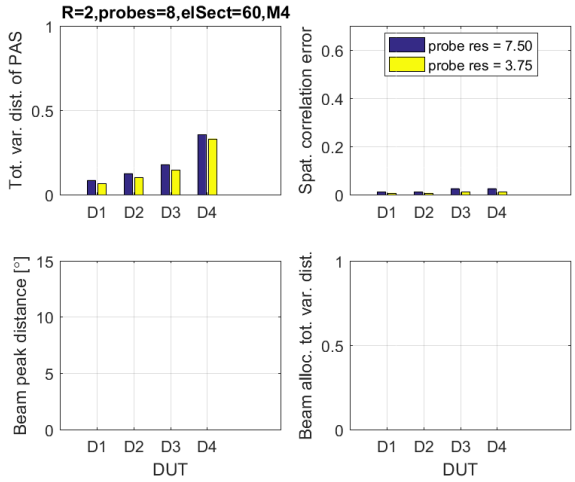

Fig. 14. Impact of probes angular spacing on performance metrics, LOS $M4$.

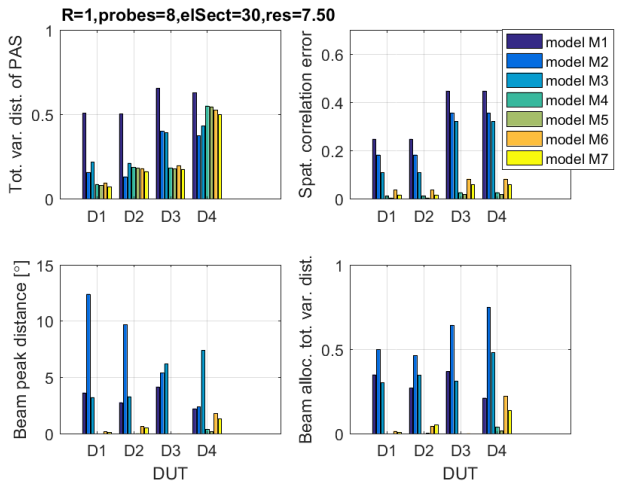

Fig. 15. Performance metrics for all models and all DUTs.

VII. Conclusions

We have discussed over-the-air performance evaluation of massive MIMO devices. Concerning test zone sizes we can conclude from the literature that for electrically large devices a straight forward extension of MPAC and the plane wave synthesis would lead to a prohibitive requirement of probe and hardware resources. Thus there is a need to develop new MPAC configurations that are suitable and cost-effective for mm-wave massive MIMO testing. We have presented a complete setup and methods to address these needs.

We have introduced four novel metrics and conducted a set of simulations in order to evaluate the setup and to determine the configuration parameters. The found recommended configuration parameters for DUTs sized up to 16×16 without displacement are as follows: range length $R = 1$ m, eight simultaneously active probes, 30° elevation sector covered by probe panels, and with 7.5° angular spacing of probes.

It could be possible to specify similar "channel model validation measurements" as in 3GPP [9], but now with the spatial correlation measurement substituted by the defined PAS based metrics. For validation purposes, the calibrated MPAC setup would be measured utilizing VNA and a linearly polarized reference antenna. A threshold for the accepted total variation distance of PAS should be set.

As a future work one could investigate deeper the joint space, time, and frequency characteristics of reference channel models and the emulation realizable with the proposed MPAC setup. Massive MIMO DUT, with a high resolution both in angular and delay domains, may resolve individual sub-paths of the reference model. It would be interesting to study the fading statistics in beam domain in both the reference case and the OTA case. The calibration procedure for practical setups is expected to be challenging at mm-wave frequencies and requires future investigations.

Acknowledgment

The part of this research performed at University of Oulu has been supported by Finnish Funding Agency for Technology and Innovation (Tekes), Nokia, Bittium, MediaTek, Kyynel, and Keysight Technologies Finland.

References

[1] J. G. Andrews, S. Buzzi, W. Choi, S. V. Hanly, A. Lozano, A. C. K. Soong, and J. C. Zhang, "What will 5G be?" *IEEE Journal on Selected Areas in Communications*, vol. 32, no. 6, pp. 1065–1082, June 2014.

[2] A. Osseiran, J. F. Monserrat, P. Marsch, M. Dohler, and T. Nakamura, Eds., *5G Mobile and Wireless Communications Technology*. Cambridge University Press, July 2016.

[3] "Technical feasibility of IMT in bands above 6 GHz," ITU-R Report M.2376-0, Tech. Rep., July 2015.

[4] "Air interface working group; verizon 5th generation radio access; physical layer procedures," Verizon 5G TF, Tech. Rep. TS V5G.213 v1.0 (2016-06), June 2016.

[5] E. G. Larsson, O. Edfors, F. Tufvesson, and T. L. Marzetta, "Massive MIMO for next generation wireless systems," *IEEE Communications Magazine*, vol. 52, no. 2, pp. 186–195, February 2014.

[6] X. Gao, O. Edfors, F. Rusek, and F. Tufvesson, "Massive MIMO performance evaluation based on measured propagation data," *IEEE Transactions on Wireless Communications*, vol. 14, no. 7, pp. 3899–3911, July 2015.

[7] T. Wirth, L. Thiele, M. Kurras, M. Mehlhose, and T. Haustein, "Massive MIMO proof-of-concept: Emulations and hardware-field trials at 3.5 GHz," in *2016 50th Asilomar Conference on Signals, Systems and Computers*, Nov 2016, pp. 1793–1798.

[8] M. Rumney, P. Cain, T. Barratt, A. L. Freire, W. Yuan, E. Mellios, and M. Beach, "Testing 5G: evolution or revolution?" in *Radio Propagation and Technologies for 5G (2016)*, Oct 2016, pp. 1–9.

[9] TR 37.977, "Evolved universal terrestrial radio access; verification of radiated multi-antenna reception performance of user equipment," 3GPP, Tech. Rep. V14.3.0, March 2017.

[10] "Test Plan for 2x2 Downlink MIMO and Transmit Diversity Over-the-Air Performance," CTIA Certification, Tech. Rep. Ver 1.0, August 2015.

[11] X. Chen, "Throughput modeling and measurement in an isotropic-scattering reverberation chamber," *IEEE Transactions on Antennas and Propagation*, vol. 62, no. 4, pp. 2130–2139, April 2014.

[12] W. Yu, Y. Qi, K. Liu, Y. Xu, and J. Fan, "Radiated two-stage method for LTE MIMO user equipment performance evaluation," *IEEE Transactions on Electromagnetic Compatibility*, vol. 56, no. 6, pp. 1691–1696, Dec 2014.

[13] P. Kyösti, T. Jämsä, and J.-P. Nuutinen, "Channel modelling for multiprobe over-the-air MIMO testing," *International Journal of Antennas and Propagation*, vol. 2012, 2012.

[14] R. Mehmood, M. A. Jensen, and J. W. Wallace, "Reconfigurable OTA chamber: A new paradigm for testing of MIMO wireless devices," in *2015 IEEE 6th International Symposium on Microwave, Antenna, Propagation, and EMC Technologies (MAPE)*, Oct 2015, pp. 591–594.

[15] 3GPP/3GPP2 TR 25.996 V6.1.0, "Spatial Channel Model for Multiple Input Multiple Output (MIMO) Simulations," 3^{rd} Generation Partnership Project, Tech. Rep., 2003.

[16] "IST-4-027756 WINNER II Deliverable 1.1.2. v.1.2, WINNER II Channel Models," IST-WINNER2, Tech. Rep., 2007.

[17] TR 38.901, "Study on channel model for frequencies from 0.5 to 100 GHz," 3GPP, Tech. Rep. V14.1.1, July 2017.

[18] A. Khatun, K. Haneda, M. Heino, L. Li, P. Kyösti, and R. Tian, "Feasibility of multi-probe over-the-air antenna test methods for frequencies above 6 ghz," in *2015 Loughborough Antennas Propagation Conference (LAPC)*, Nov 2015, pp. 1–5.

[19] D. Reed, A. Rodriguez-Herrera, and R. Borsato, "Measuring massive MIMO array systems using over the air techniques," in *The 11th European Conference on Antennas and Propagation (EuCAP 2017)*, March 2017.

[20] P. Kyösti, J. Kyröläinen, and W. Fan, "Assessing measurement distances for OTA testing of massive MIMO base station at 28 GHz," in *2017 11th European Conference on Antennas and Propagation (EUCAP)*, March 2017, pp. 3679–3683.

[21] W. Fan, I. Carton, P. Kyösti, A. Karstensen, T. Jämsä, M. Gustafsson, and G. F. Pedersen, "A step toward 5G in 2020: Low-cost OTA performance evaluation of massive MIMO base stations." *IEEE Antennas and Propagation Magazine*, vol. 59, no. 1, pp. 38–47, Feb 2017.

[22] P. Kyösti, W. Fan, G. F. Pedersen, and M. Latva-aho, "On dimensions of OTA setups for massive MIMO base stations radiated testing," *IEEE Access*, vol. PP, no. 99, pp. 1–1, 2016.

[23] W. A. T. Kotterman, C. Schirmer, M. H. Landmann, and G. Del Galdo, "New challenges in over-the-air testing," in *2017 11th European Conference on Antennas and Propagation (EUCAP)*, March 2017, pp. 3676–3678.

[24] M. D. Foegelle, "The future of MIMO over-the-air testing," *IEEE Communications Magazine*, vol. 52, no. 9, pp. 134–142, September 2014.

[25] C. Schirmer, M. H. Landmann, W. A. T. Kotterman, M. Hein, R. S. Thomä, G. D. Galdo, and A. Heuberger, "3D wave-field synthesis for testing of radio devices," in *The 8th European Conference on Antennas and Propagation (EuCAP 2014)*, April 2014, pp. 3394–3398.

[26] J. T. Toivanen, T. A. Laitinen, V. M. Kolmonen, and P. Vainikainen, "Reproduction of arbitrary multipath environments in laboratory conditions," *IEEE Transactions on Instrumentation and Measurement*, vol. 60, no. 1, pp. 275–281, Jan 2011.

[27] A. Khatun, T. Laitinen, V.-M. Kolmonen, and P. Vainikainen, "Dependence of error level on the number of probes in over-the-air multiprobe test systems," *International Journal of Antennas and Propagation*, vol. 2012, p. 6, March 2012.

[28] J. E. Hansen, *Spherical Near-Field Antenna Measurements*. London, England: Peter Peregrinus Ltd., 1988.

[29] A. Khatun, V. M. Kolmonen, V. Hovinen, D. Parveg, M. Berg, K. Haneda, K. I. Nikoskinen, and E. T. Salonen, "Experimental verification of a plane-wave field synthesis technique for MIMO OTA antenna

testing," *IEEE Transactions on Antennas and Propagation*, vol. 64, no. 7, pp. 3141–3150, July 2016.

[30] "METIS Channel Models, Deliverable D1.4 v.1.3," ICT-317669 METIS project, Tech. Rep., 2015.

[31] P. Kyösti, J. Nuutinen, and T. Jämsä, "MIMO OTA test concept with experimental and simulated verification," *in Proc. of the 4th European conference on antennas and propagation, EuCAP 2010, Barcelona, Spain*, April 2010.

[32] C. Schirmer, R. D. M. Lorenz, W. A. T. Kotterman, G. D. Galdo, A. Heuberger, and M. H. Landmann, "A calibration procedure for practical wave-field synthesis in over-the-air testing," in *IC1004 TD(15)13026*, May 2015.

[33] P. Stoica and R. L. Moses, *Spectral analysis of signals*. Pearson/Prentice Hall Upper Saddle River, NJ, 2005.